THE SZEWALSKI INSTITUTE OF FLUID-FLOW MACHINERY
POLISH ACADEMY OF SCIENCES

TRANSACTIONS OF THE INSTITUTE OF FLUID-FLOW MACHINERY

119

GDAŃSK 2007

TRANSACTIONS OF THE INSTITUTE OF FLUID-FLOW MACHINERY Appears since 1960

Aims and Scope

Transactions of the Institute of Fluid-Flow Machinery have primarily been established to publish papers from four disciplines represented at the Institute of Fluid-Flow Machinery of Polish Academy of Sciences, such as:

- Liquid flows in hydraulic machinery including exploitation problems,
- Gas and liquid flows with heat transport, particularly two-phase flows,
- Various aspects of development of plasma and laser engineering,
- Solid mechanics, machine mechanics including exploitation problems.

The periodical, where originally were published papers describing the research conducted at the Institute, has now appeared to be the place for publication of works by authors both from Poland and abroad. A traditional scope of topics has been preserved.

Only original and written in English works are published, which represent both theoretical and applied sciences. All papers are reviewed by two independent referees.

EDITORIAL AND PUBLISHING OFFICE

IFFM Publishers (Wydawnictwo IMP), The Szewalski Institute of Fluid Flow Machinery, Fiszera 14, 80-952 Gdańsk, Poland, Tel.: +48(58)6995141, Fax: +48(58)3416144, E-mail: esli@imp.gda.pl; now@imp.gda.pl http://www.imp.gda.pl/

Terms of subscription

Subscription order and payment should be directly sent to the Publishing Office

Warunki prenumeraty w Polsce

Wydawnictwo ukazuje się przeciętnie dwa lub trzy razy w roku. Cena numeru wynosi 25,- zł. Zamówienia z określeniem okresu prenumeraty, nazwiskiem i adresem odbiorcy należy kierować bezpośrednio do Wydawcy (Wydawnictwo IMP, Instytut Maszyn Przepływowych PAN, ul. Gen. Fiszera 14, 80-952 Gdańsk; e-mail: now@imp.gda.pl). Osiągalne są również wydania poprzednie.
Prenumerata jest również realizowana przez jednostki kolportażowe RUCH S.A. właściwe dla miejsca zamieszkania lub siedziby prenumeratora.

Articles in *Transactions of the Institute of Fluid-Flow Machinery* are abstracted and indexed within:

INSPEC Database;
Energy Citations Database;
Applied Mechanics Reviews;
Abstract Journal of the All-Russian Inst. of Sci. and Tech. Inf. VINITI.

ISSN 0079-3205

TRANSACTIONS OF THE INSTITUTE OF FLUID-FLOW MACHINERY

No. 119, 2007, 29-38

MARIUSZ JASIŃSKI*, MARCIN GOCH, ZENON ZAKRZEWSKI, JERZY MIZERACZYK

Microwave microdischarges of low-power at atmospheric pressure

Centre for Plasma and Laser Engineering, The Szewalski Institute of Fluid-Flow Machinery, Polish Academy of Sciences, Fiszera 14, 80-952 Gdańsk, Poland

Abstract

In this paper we present a simple and cheap microwave (2.45 GHz) source of microdischarges in argon and neon at atmospheric pressure. The source consisted of a cheap 2.45 GHz microwave magnetron generator and 50 Ω coaxial line terminated with a simple coaxial plasma applicator. The new microwave source of microdischarges operated stable in the form of a small plasma jet at absorbed microwave powers of 9–80 W and gas flow rates of 0.5–25 l/min. The length and diameter of plasma jets were 1.5–14 mm and 0.5–1.5 mm, respectively, depending on the kind of gas, gas flow rate and microwave power absorbed by the discharge. The temperature of the plasma jets could be changed from 30°C to 1200°C by changing the gas flow rate or/and absorbed microwave power. The electron density in the plasma jet was around $3 \cdot 10^{14}$ cm^{-3}–$1.1 \cdot 10^{15}$ cm^{-3}, depending on the discharge conditions.

Keywords: Microwave discharges; Microplasma; Atmospheric pressure microplasma

1 Introduction

Nowadays, there is a growing interest in microplasma sources. There are many different factors defining the usefulness of microplasma: economics, portability, easy to use, less operation costs and small size. Microdischarges at atmospheric pressure, having dimensions in the range from μm to mm, find practical applications in various fields such as gas cleaning systems, microwelding, surface modification [1], light sources (visible [2] and UV sources [3]), atomic spectroscopy system [4, 5]. They can also find the use in the biomedical applications such as sterilization of medical instruments and bio-MEM's [6, 7], high-precision surgery [8],

*Corresponding author. E-mail address: mj@imp.gda.pl

cells treatment and deactivation of bacteria and viruses [9]. There are few types of microplasma sources: microhollow cathodes dc discharges [10, 11], dielectric barrier discharges [12, 13], RF discharges [14], and microwave discharges [15]. Microwave excited microplasmas feature long lifetime and simplicity compared to other microplasma systems.

In this paper we present a microwave excited source of microdischarges in argon and neon at atmospheric pressure. The main advantage of the presented microwave source is its simplicity and low cost. The simplicity of the device and stability of the microdischarge jet allow for the concluding that the microwave microdischarge source can find practical applications in various fields mentioned above.

2 Experimental setup

Figure 1 shows the essential components of the experimental setup. It consists of a microwave magnetron generator (2.45 GHz), microwave power measuring system (directional coupler, incident and reflected power meters), microwave coaxial plasma applicator and gas flow control system. The microwave components were connected with coaxial cables (50 Ω).

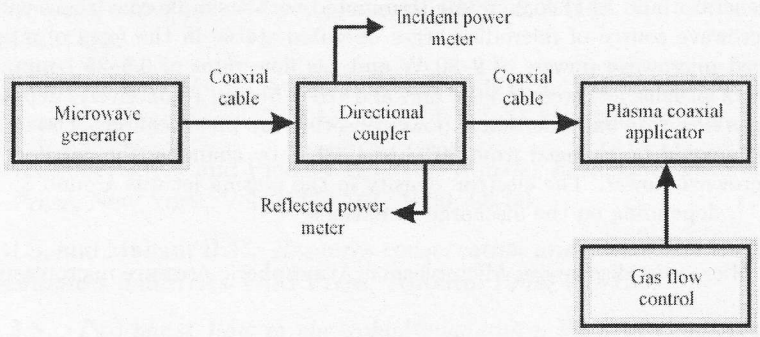

Figure 1. Diagram of the experimental setup.

In our investigations either argon or neon at atmospheric pressure were used as a working gas. The gas flow rates ranged from 0.5 to 25 l/min. The discharges were sustained at 2.45 GHz with an absorbed microwave power from 9 to 80 W. The sketch and photo of the coaxial applicator are shown in Figs. 2a and b. The structure of the applicator was based on the coaxial line and consisted of a copper wire ($\phi = 1$ mm) with a sharpened tip confined with a polyamide tube (the inner diameter ID = 4 mm, the outer diameter OD = 6 mm). The lengths of the copper wire and the surrounded polyamide tube were the same. The applicator was connected with a coaxial cable by using N-type connector.

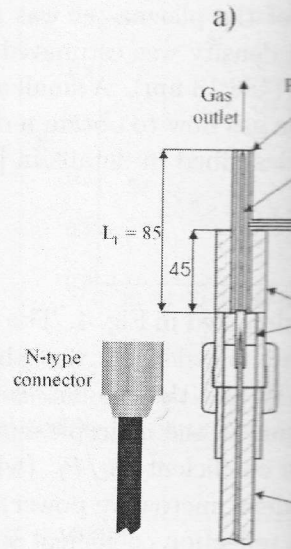

Figure 2. The cross-sectional view (a) microdischarges operated at diameters of the polyamide t L_t was 85 mm.

The optimum length L_t of the co The arrow shown in Fig. 3 depic lowest reflected microwave power

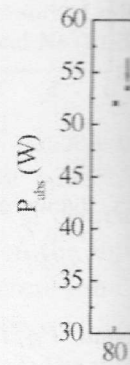

Figure 3. Dependence of the absorbed rate $Q = 1$ l/min, incident po

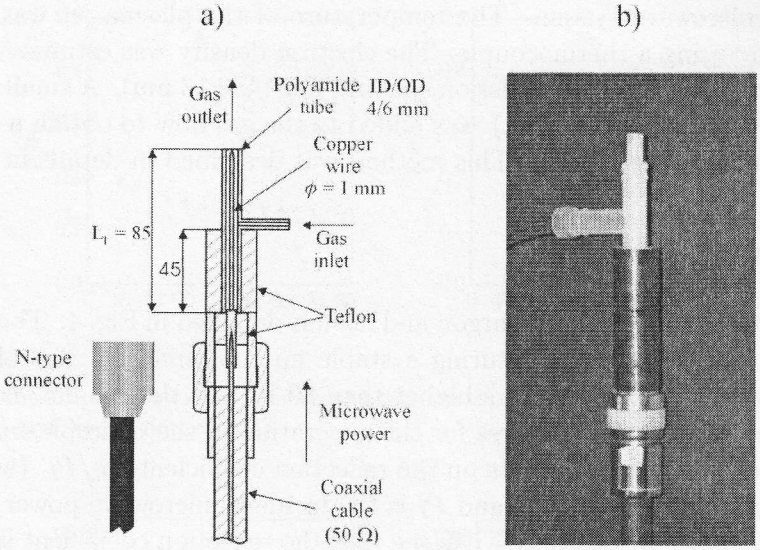

Figure 2. The cross-sectional view (a) and the photo (b) of the 2.45 GHz microwave source of microdischarges operated at atmospheric pressure. The inner (ID) and outer (OD) diameters of the polyamide tube were 4 and 6 mm, respectively. The applicator length L_t was 85 mm.

The optimum length L_t of the coaxial applicator was chosen according to Fig. 3. The arrow shown in Fig. 3 depicts the best matching of the applicator (i.e. the lowest reflected microwave power), and hence the optimum applicator length L_t.

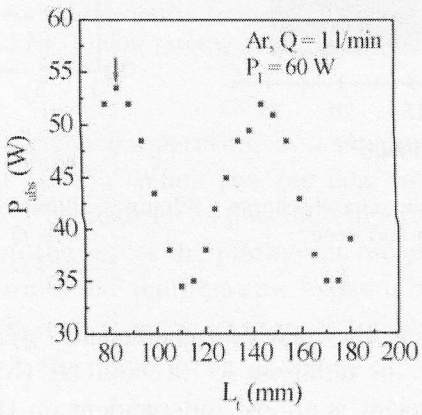

Figure 3. Dependence of the absorbed microwave power P_{abs} on the applicator length L_t. Flow rate $Q = 1$ l/min, incident power $P_I = 60$ W.

Apart from this matching, no other impedance matching circuits were used in the presented microwave system. The temperature of the plasma jet was measured at its top by using a thermocouple. The electron density was estimated from the Stark broadening of the H_β emission spectral line (486.13 nm). A small amount of water vapour (about 0.1 % vol.) was added to the gas flow to obtain a detectable intensity of H_β emission line. This method was described in details in [16].

3 Results

The area of stable operation in argon and neon is depicted in Fig. 4. The minimum absorbed microwave power ensuring a stable microplasma jets was about 9 W. The absorbed microwave powers higher than 80 W and the gas flow rates higher than 25 l/min seem to be useless for the generation of the microplasmas.

Influence of the gas flow rate on the reflection coefficient P_R/P_I (where P_R is the reflected microwave power and P_I is the incident microwave power) for argon and neon is shown in Fig. 5. We can see that the reflection coefficient is relatively low and almost constant in the wide range of gas flow rates.

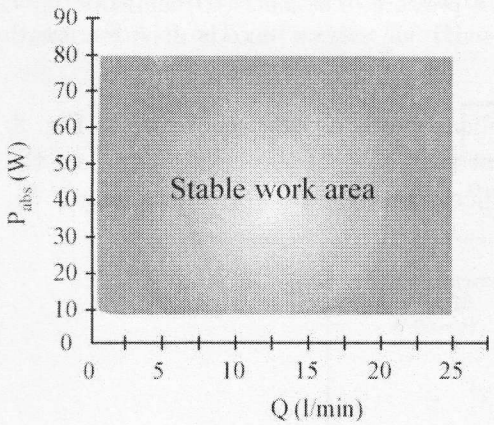

Figure 4. The area of stable microdischarge operation in argon and neon.

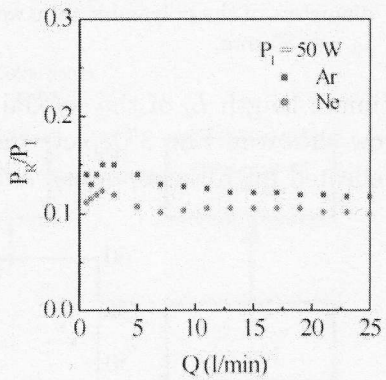

Figure 5. Influence of the Ar and Ne flow rates Q on the reflection coefficient P_R/P_I.

Figures 6a and b show the reflection coefficient P_R/P_I as a function of incident microwave power for different Ar (a) and Ne (b) flow rates. It is seen that the reflection coefficient is almost independent on the discharge conditions. Figures 7a and b show the temperature on the top of the plasma jet as a function of absorbed microwave power for different Ar (a) and Ne (b) flow rates, respectively. The plasma temperature of argon microdischarge is about 1.25 times higher than the temperature of neon microdischarge.

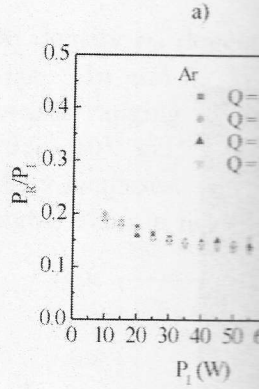

Figure 6. Influence of the incident mic (a) and Ne (b) flow rates Q

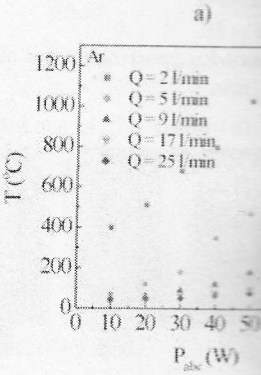

Figure 7. Influence of the absorbed mi different Ar (a) and Ne (b) f

We can control the plasma t the absorbed microwave power. absorbed microwave power decrea temperature measured on the top The wide range of microplasma microplasma applications.

As shown in the Fig. 8, the mi of a skin.

The microplasma jet appeara Figs. 9 and 10. The microplasma zones: an inner core and an outer sions of plasma jets can be chang

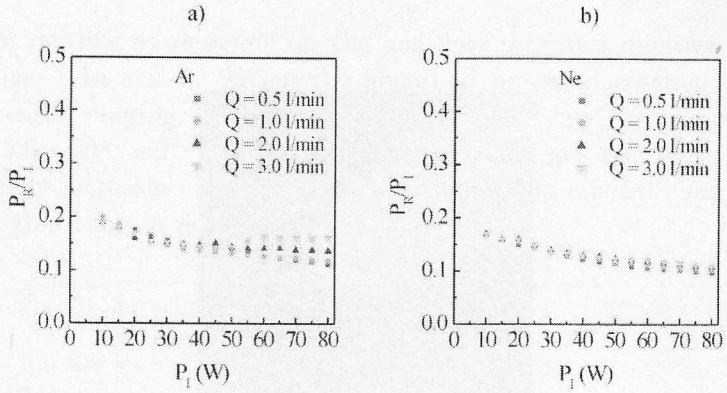

Figure 6. Influence of the incident microwave power on the reflection coefficient for different Ar (a) and Ne (b) flow rates Q.

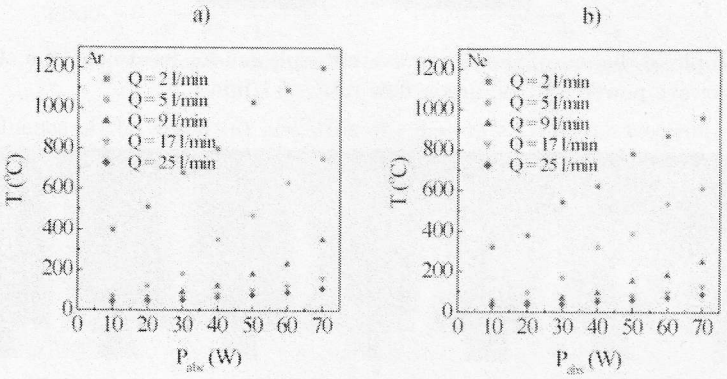

Figure 7. Influence of the absorbed microwave power on the temperature of the plasma jet for different Ar (a) and Ne (b) flow rates Q.

We can control the plasma temperature by changing the gas flow rate and the absorbed microwave power. When the gas flow rate increases and/or the absorbed microwave power decreases, the plasma temperature decreases. The gas temperature measured on the top of the plasma jet ranged from 30°C to 1200°C. The wide range of microplasma temperature expands the range of microwave microplasma applications.

As shown in the Fig. 8, the microdischarge source can be applied for treatment of a skin.

The microplasma jet appearance for different gas flow rates are presented in Figs. 9 and 10. The microplasma jets resemble a candle flame with two distinct zones: an inner core and an outer shell. According to Figs. 9 and 10, the dimensions of plasma jets can be changed by choosing the gas flow rate.

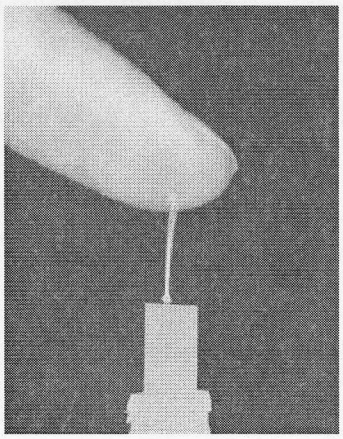

Figure 8. Example of the use of the microwave microplasma for treatment of a skin. Absorbed microwave power – 10 W, argon flow rate – 5 l/min

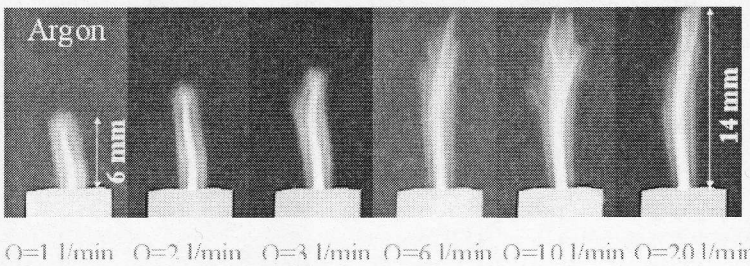

Figure 9. Influence of the Ar flow rate Q on the plasma jet length for an absorbed microwave power $P_{abs} = 30$ W.

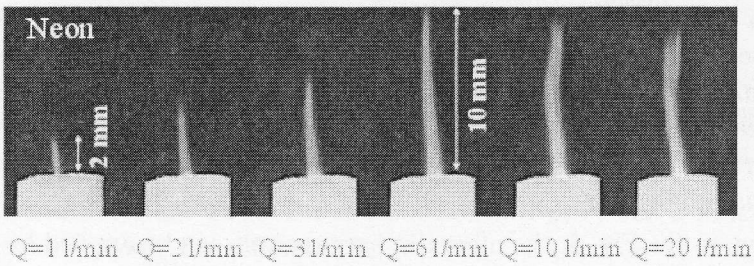

Figure 10. Influence of the Ne flow rate Q on the plasma jet length for an absorbed microwave power $P_{abs} = 30$ W.

The electron density n_e depends
shown in Figs. 11a and b. Wh
density increases ranging from 7
$3 \cdot 10^{14}$ to $5.5 \cdot 10^{14}$ cm^{-3} at n
electron density increases. The el
two times higher than in neon.

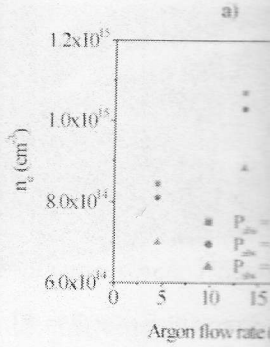

Figure 11. Influence of the argon (a) a
different microwave absorbe

Figure 12. Sketch of the

The electron density n_e depends on the gas flow rate and microwave power as shown in Figs. 11a and b. When the absorbed power increasing, the electron density increases ranging from $7 \cdot 10^{14}$ to $1.1 \cdot 10^{15}$ cm^{-3} at argon and from $3 \cdot 10^{14}$ to $5.5 \cdot 10^{14}$ cm^{-3} at neon. With increasing gas flow rate, the level of electron density increases. The electron density in argon microdischarges is about two times higher than in neon.

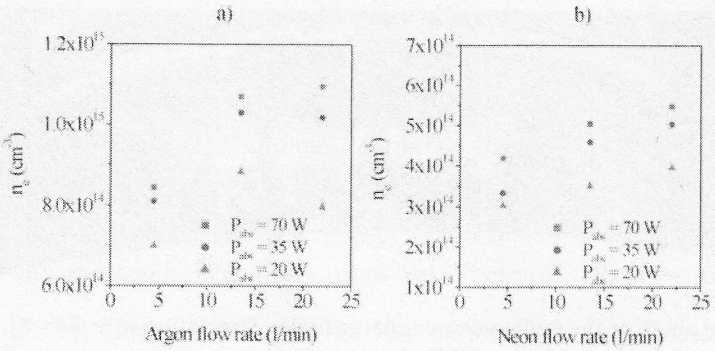

Figure 11. Influence of the argon (a) and neon (b) flow rate Q on the electron density n_e for different microwave absorbed power.

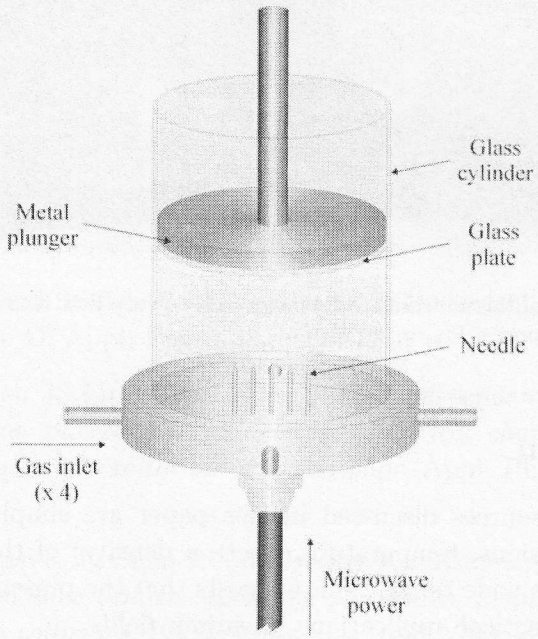

Figure 12. Sketch of the multi-microdischarge microwave source.

We proposed a method of microplasma generation based on multi-microdischarge source (Fig. 12) at atmospheric pressure. The multi-microdischarge microwave source consists of a glass cylinder, which contains few needles and a movable metal plunger terminated with a glass plate. Figure 13 and 14 present microwave multi-microdischarges in argon and neon, respectively. In this case the distance between needles and plunger was about 1 mm.

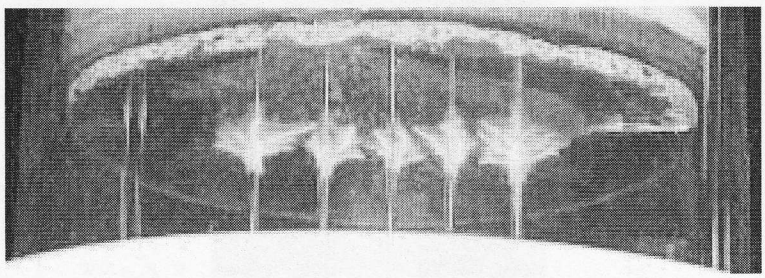

Figure 13. The photo of the multi-microdischarge in Ar. Argon flow rate $Q = 4$ l/min, absorbed microwave power $P_{abs} = 20$ W.

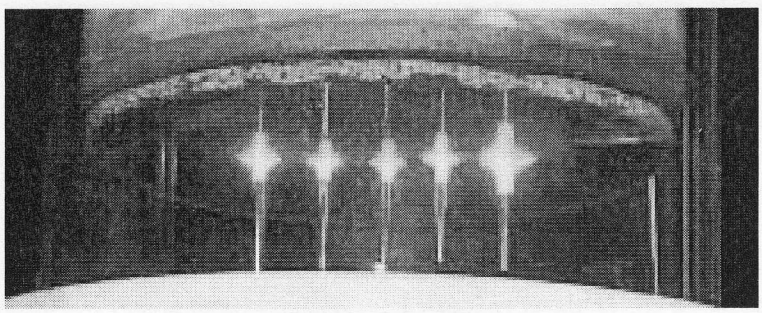

Figure 14. The photo of the multi-microdischarge in Ne. Neon flow rate $Q = 4$ l/min, absorbed microwave power $P_{abs} = 20$ W.

4 Conclusion

The microplasma sources discussed in this paper are simple and cheap. The parameters (dimensions, temperature, electron density) of the microplasma jets can be changed in a wide range. This suggests that the presented microdischarge sources can find practical applications in various fields.

The paper presents overall characteristics of the new microwave plasma source of microdicharges. Detailed interpretation will follow later.

Received 20 November 2006

References

[1] Kim J. and Terashima K.: *pressure microplasmas for* 2005, 324.

[2] Iza F. and Hopwood J.: *Spli plasma impedance and pow* 2005, 397.

[3] Kikuchi T., Hasegawa Y. an *pressure: characterization a* Appl. Phys., 37, 2004, 1537.

[4] Stonies R., Schermer S.,. V *crowave plasma torch*, Plasm

[5] . Bilgic A. M, Engel U., V *A new low-power microwave atomic emission spectrometr*

[6] Iza F. and. Hopwood J. A: *R of a microwave-frequency mi* 32, 2004, 2.

[7] Iza F. and Hopwood J. A.: *microstrip split-ring resonat*

[8] Stalder K. R., McMillen D. Phys. D: Appl. Phys., 38, 20

[9] Sladek R.E.J. and Stoffels E. *needle*, J. Phys. D: Appl. Ph

[10] Park S. J., Chen J., Liu C. *arrays of silicon microdisch* (30×30) *arrays and excitat* 419.

[11] Kurunczi P., Lopez J., Shah *pressure microhollow cathode energy electron collisions*, Int

[12] Miclea M., Kunze K., Musa *barrier discharge – a powerful* Spectrochim. Acta B, 56, 200

References

[1] Kim J. and Terashima K.: *Microwave excited nonequilibrium atmospheric pressure microplasmas for polymer surface modification*, Proc. APSPT-4 2005, 324.

[2] Iza F. and Hopwood J.: *Split-ring resonator microplasma: microwave model, plasma impedance and power efficiency*, Plasma Sources Sci. Technol., 14, 2005, 397.

[3] Kikuchi T., Hasegawa Y. and Shirai H.: *RF microplasma jet at atmospheric pressure: characterization and application to thin film processing*, J. Phys. D: Appl. Phys., 37, 2004, 1537.

[4] Stonies R., Schermer S.,. Voges E and Broekaert J.A.C.: *A new small microwave plasma torch*, Plasma Sources Sci. Technol., 13, 2004, 604.

[5] . Bilgic A. M, Engel U., Voges E., Kuckelheim M. and Broekaert J.A.C.: *A new low-power microwave plasma sources using microstrip technology for atomic emission spectrometry*, Plasma Sources Sci. Technol., 9, 2000, 1.

[6] Iza F. and. Hopwood J. A: *Rotational, vibrational, and excitation temperature of a microwave-frequency microplasma*, IEEE Transaction on Plasma Science, 32, 2004, 2.

[7] Iza F. and Hopwood J. A.: *Low-power microwave plasma source based on a microstrip split-ring resonator*, IEEE Trans. on Plasma Science, 31, 2003, 4.

[8] Stalder K. R., McMillen D. F. and Woloszko J.: *Electrosurgical Plasmas*, J. Phys. D: Appl. Phys., 38, 2005, 1728.

[9] Sladek R.E.J. and Stoffels E.: *Deactivation of* Escherichia coli *by the plasma needle*, J. Phys. D: Appl. Phys., 38, 2005, 1716.

[10] Park S. J., Chen J., Liu C. and Eden J. G.: *Independently addressable subarrays of silicon microdischarge devices: electrical characteristics of large* (30×30) *arrays and excitation of a phosphor*, Appl. Phys. Lett., 78, 2001, 419.

[11] Kurunczi P., Lopez J., Shah H. and Becker K.: *Excimer formation in high-pressure microhollow cathode discharge plasmas in helium initiated by low-energy electron collisions*, Int. J. Mass Spectrom., 205, 2001, 277.

[12] Miclea M., Kunze K., Musa G., Franzke J. and Niemax K.: *The dielectric barrier discharge – a powerful microchip plasma for diode laser spectrometry*, Spectrochim. Acta B, 56, 2001, 37.

[13] Brandenburg R., Wagner H. E.,. Morozov A. M and Kozlov K. V.: *Axial and radial development of the microdischarges of barrier discharges in N_2/O_2 mixtures at atmospheric pressure*, J. Phys. D: Appl. Phys., 38, 2005, 1649.

[14] Ichiki T., Koidesawa T. and Horiike Y.: *An atmospheric-pressure microplasma jet source for the optical emission spectroscopic analysis of liquid sample*, Plasma Sources Sci. Technol., 12, 2003, 16.

[15] Schermer S., Bings N. H.,. Bilgic A. M, Stonies R., Voges E. and Broekaert J.A C.: *An improved microstrip plasma for optical emission spectrometry of gaseous species*, Spectrochim. Acta B, 58, 2003, 1585.

[16] Jasiński M., Mizeraczyk J. and Zakrzewski Z.: *Spectroscopic measurements of electron density in microwave torch discharge at atmospheric pressure*, Frontiers in Low Temperature Plasma Diagnostics VI, Les Houches, France, April 17-21, 2005, EP6-1-4.

S

Laser diagnostics of
in DC positive s

Dept. of Electrical and
700 Danno

The streamer observation and LIF det
formed during the steady-state positive
relationship between the regular strea
streamer was explained for no time sync
shower reactor, two-dimensional distrib
only in the discharge zone but also bo
reactor. The presence of the ground-s
in DC streamer discharge was also inv
(EHD) flow on NO profiles in the react
discussed. The obtained results showe
in the plasma region formed by the cor
but also in the upstream region of the
cals were generated and stayed mainly
electrodes.

Keywords: Laser-induced fluorescence

1 Introduction

Streamer discharge induced plas
pressure non-thermal plasmas use
To produce streamers pulsed coro
For the moment DC corona discha
mercially available technique for

*E-mail address: skana@cc.oita-u.ac.j

TRANSACTIONS OF THE INSTITUTE OF FLUID-FLOW MACHINERY

No. 119, 2007, 39-54

SEIJI KANAZAWA*

Laser diagnostics of NO molecules and OH radicals in DC positive streamer corona discharges

Dept. of Electrical and Electronic Engineering, Oita University,
700 Dannoharu, Oita, 870-1192 Japan

Abstract

The streamer observation and LIF detection of the NO molecules and OH radicals were performed during the steady-state positive DC corona discharge at atmospheric pressure. The time relationship between the regular streamer coronas, laser pulse, LIF signal and laser-induced streamer was explained for no time synchronization LIF measurement. Using the corona radical shower reactor, two-dimensional distributions of ground-state NO ($X^2\Pi$) could be observed not only in the discharge zone but also both in the downstream and the upstream regions of the reactor. The presence of the ground-state OH ($X^2\Pi$) and excited-state OH ($A^2\Sigma^+$) radicals in DC streamer discharge was also investigated. Moreover, the effect of electrohydrodynamic (EHD) flow on NO profiles in the reactor and ozone interference in OH LIF measurement were discussed. The obtained results showed that the density of NO molecules decreased not only in the plasma region formed by the corona streamers and the downstream region of the reactor but also in the upstream region of the reactor. On the other hand, the ground-state OH radicals were generated and stayed mainly in the region where streamers propagated between the electrodes.

Keywords: Laser-induced fluorescence; NO, OH radical; DC streamer corona discharge

1 Introduction

Streamer discharge induced plasma is one of the most efficient atmospheric-pressure non-thermal plasmas used for the treatment of many gaseous pollutants. To produce streamers pulsed corona discharges have been used extensively [1, 2]. For the moment DC corona discharge was evaluated to be cost effective and commercially available technique for producing streamers in larger electrodes gap

*E-mail address: skana@cc.oita-u.ac.jp

distance (> 5 cm). Especially corona radical shower system which uses DC streamers, has been developed and its performance evaluated for NO_x removal [3, 4].

In a streamer the energetic electrons collide with the gas molecules and produce radicals, resulting in the enhancement of plasma chemical reactions. Among many radicals, OH radical plays an important role in the kinetics of plasma chemical process. Therefore, the relationship between the streamers and radicals in non-thermal plasma reactors is of great interest as well as the treatment process of harmful gas molecules. Recently, in order to understand the process occurring in the non-thermal plasmas, the time- and space-resolved discharge observation using an intensifier-gated charge-coupled devise (ICCD) camera and harmful gas molecule and active radical measurements by laser-induced fluorescence (LIF) technique based on tunable pulsed lasers have been applied as the state-of-the-art optical diagnostics [1, 2, 5-21]. The LIF measurements performed in non-thermal plasmas for the application of pollution control are summarized in Table I. Up to now, various species such as OH radical, NO molecule, and O atom have been measured [5-19]. In the measurement using pulsed discharge, the measurement was performed after the discharge in either the single or the low-repetition pulsed discharges to avoid the emission from the intensive discharges.

In this paper, the characteristics of positive DC streamer coronas and NO removal process together with OH radical dynamics in corona radical injection or radical shower system are described. Our investigation was aimed at measuring the NO molecules and OH radicals during the steady-state DC corona discharge condition. This is an essential difference to the investigations for pulsed discharges in which the LIF monitoring of these species was carried out after the single transient discharge.

2 Experimental apparatus and methods

Figure 1 shows the schematic diagram of the experimental setup. The apparatus with laser system and fundamentals of the measuring techniques have been described in detail elsewhere [10, 17, 18] and only a brief description is given in this paper. In order to observe the ground-state NO profiles in the reactor by LIF technique, NO $[A^2\Sigma^+(v' = 0) \rightarrow X^2\Pi(v'' = 0)]$ system at 226nm was used and almost full band of the fluorescence signal was detected. For monitoring the ground-state OH radicals, the scheme with excitation at 282 nm $[A^2\Sigma^+(v' = 1) \leftarrow X^2\Pi(v'' = 0)]$ and detection at 309 nm $[A^2\Sigma^+(v' = 0) \rightarrow X^2\Pi(v'' = 0)]$ was used. These UV laser beams were generated by a laser system consisted of XeF excimer laser (Lambda Physik, COMPex 150), dye laser (Lambda Physik, SCANmate) and BBO crystal. LIF signal emitted was imaged onto a gated ICCD camera (LaVision, Flame Star

II or Andor, iStar). For the 2-D observation between the electrodes with a 30-mm or 50 mm-gap, a laser sheet (1 mm-width and 25 mm or 35 mm-height) was used. In addition to these measurements, in the case of time-resolved OH radical detection, LIF signal emitted at 90 degree to the laser beam was focused onto the entrance slit of a 25 cm monochromator (Nikon, P-250) through a lens. The LIF signal detected by a photomultiplier tube (PMT) was sent to a digital oscilloscope (Osc1) through a preamplifier. In addition, normal discharge emission was observed by using the ICCD camera and emission spectrum was measured by the monochromator system.

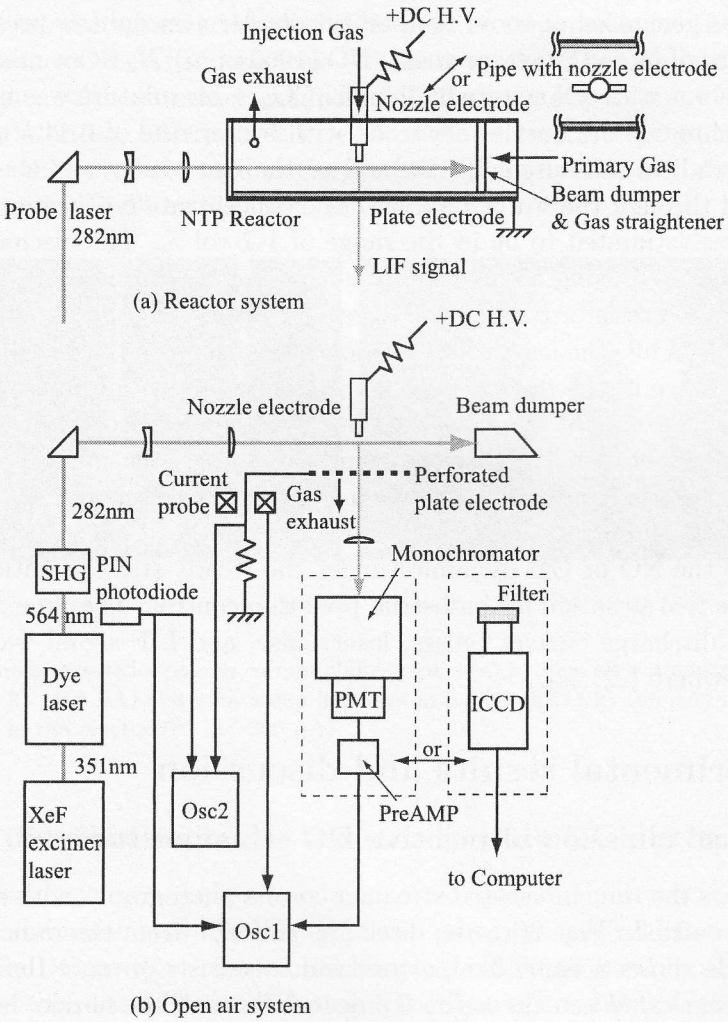

Figure 1. Schematic diagram of the experimental apparatus.

A stainless-steel pipe with a nozzle (1.0 mm in inner diameter, 1.5 mm in outer diameter) was used as the stressed electrode of the radical injection system. The gap distance was 30 mm. While, a pipe with two nozzles-to-plate electrode system, having an electrode gap of 50 mm was used as the stressed electrode of corona radical shower system. In both discharging electrodes, an additional gas (argon or CO_2 + air) could be supplied to the discharge zone through the nozzles. As a grounded electrode, the plate electrode was used in a reactor system as shown in Fig. 1(a). While, the plate electrode (100 mm in square) with an array of holes (1.5 mm in diameter) was used to allow the gas exhaust in open air system as shown in Fig. 1(b). DC high voltage with positive polarity was applied through a 10 MΩ resistor to the stressed electrode and the DC positive corona discharge was generated at room temperature under atmospheric pressure.

In the case of NO LIF measurement, NO (1000 ppm)/N_2 + air mixture flowed along the reactor with a flow rate of 3l/min. CO_2 + air mixture was injected into the reactor through the nozzles electrode with a flow rate of 0.44 l/min. In the case of OH radical measurement, instead of the use of dry air, the humid air was supplied through the water bubbler. The concentration of water around the electrodes was estimated to be in the range of 1-2 vol.%. The discharge current pulse was measured using a current probe (Pearson Electronics, 2877). Also the potential across a resistor connected between the plane electrode and the ground was measured. While the laser shot was monitored using a PIN photodiode placed at 2 m in advance of the discharge zone. A time relationship between discharge current and the laser shot was measured by another oscilloscope (Osc2). No time synchronization between the discharge and laser shot was made. This means that a laser pulse is irradiated at random between the discharge current pulses. Namely, all measurements were carried out during the discharge, therefore we can evaluate the NO or OH dynamics under the steady-state condition which is similar to the real situation for industrial pollution control. The time relationship between the discharge current pulses, laser pulse, and LIF signal was described in detail elsewhere [22, 23].

3 Experimental results and discussion

3.1 Optical emission of positive DC streamer coronas

Figure 2 shows the time integrated streamer corona photographs with an exposure time of 8 seconds. In Fig. 2(a), the discharge emission from the radical injection type electrode shows a flame like pattern which consists of more than ten thousands of streamers. When the argon is injected through the nozzle, however, the discharge pattern changes to a filament and emission become more intensive as shown in an inset of Fig. 2(a). The corona radical shower generates the differ-

ent discharge pattern due to the electrode configuration as shown in Fig. 2(b). The characteristics of DC streamer corona such as streamer velocity, its diameter, current pulse, repetition rate and so on were described in [24]. Figure 3 shows the optical emission spectra of discharges in the case of Fig. 2(a) without and with argon injection. In both discharges generated in open air, N_2 second positive band ($C^3\Pi_u \rightarrow B^3\Pi_g$) is mainly observed in the range 300-400 nm. However, it should be noted that the OH emission ($A^2\Sigma^+ \rightarrow X^2\Pi$, 0-0) is observed only in the filamentary discharge produced by argon injection. In pulsed corona discharge, OH emission has been observed and the excited state OH ($A^2\Sigma^+$) radicals decreases exponentially with increasing the oxygen [25]. It is considered that not only the different discharge pattern relating to the current density, but also the gas mixture existed between the electrodes may be responsible for the presence of the excited-state OH ($A^2\Sigma^+$) radicals. In the case of DC corona in air, the lower current density in the streamer channel may affect the population of OH ($A^2\Sigma^+$) radicals. In addition, OH radicals in excited-states are rapidly quenched by collisions with ambient gases such as oxygen [26]. The presence of the ground-state OH ($X^2\Pi$) radicals will be discussed in detail later.

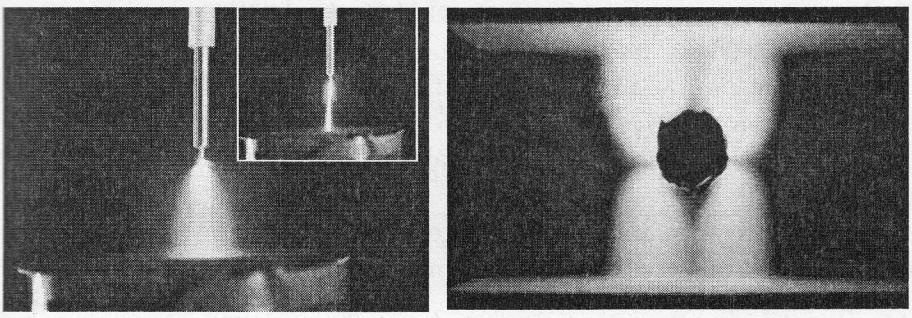

(a) (b)

Figure 2. Time integrated streamer corona photographs; (a) in open air without argon injection (29 kV, 150 μA) and with argon injection at 0.3 l/min (11 kV, 40 μA) in an inset and (b) in the reactor (30 kV, 300 μA).

3.2 NO distribution under the steady-state DC discharge condition

In the LIF measurements, as the UV laser pulse induces additional streamers during stable DC streamer corona discharge, the light emitted by the streamers can interfere with the LIF signal during NO LIF measurement. From the results of our previous measurements [22, 23], Fig. 4 shows the schematic illustration of the time relationship between the regular streamers, laser pulse, laser-induced

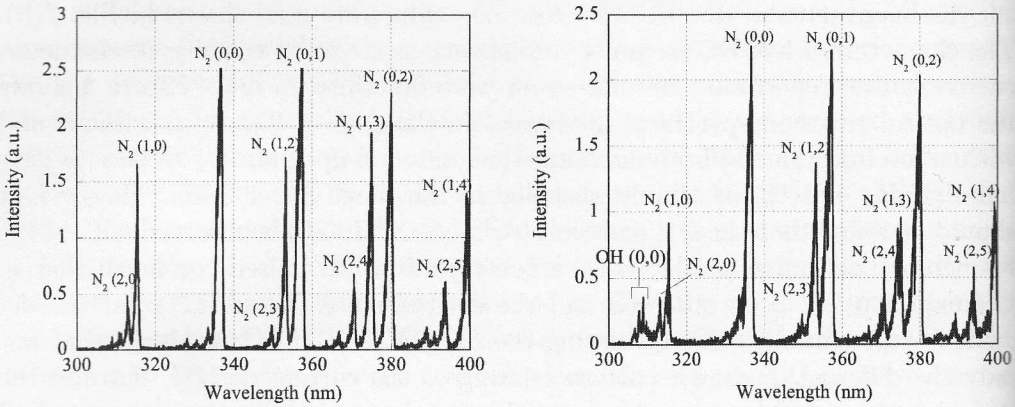

Figure 3. Optical emission spectra; (a) without argon injection (29 kV, 150 μA) and (b) with argon injection at 0.3 l/min (11 kV, 40 μA).

streamer and LIF signal. The LIF signal appears almost immediately after the laser pulse and lasts over about 30-40 ns, while the laser-induced streamers usually start later (about 35-300 ns after the laser pulse depending on the position of the laser beam in the gap) and last over about up to 500 ns as shown in Fig. 4. Consequently, an appropriate adjusting for the delay and exposure time of the ICCD camera enabled to capture the LIF signal and laser-induced streamer emission independently.

Figure 5 shows two-dimensional images of NO concentration in the reactor. Initial NO concentration is about 100 ppm. The images were taken after the NO concentration in the reactor reached a steady-state. Each image is an average of 50 captured images. The color of the images corresponds to NO spatial concentrations. As the applied voltage increases, NO LIF signal becomes weaker compared with that of the no applied voltage, indicating the decrease of NO concentration. In this case, NO is mainly converted to NO_2 via the oxidation reactions

$$NO + O + M \rightarrow NO_2 + M, \tag{R1}$$

$$NO + O_3 \rightarrow NO_2 + O_2. \tag{R2}$$

where M is a third body.

The increase of NO_2 concentration was confirmed at the reactor outlet by the measurement using the NOx monitor. Figure 6 shows the NO density profiles along the treatment gas flow. They correspond to the NO concentration along the middle line of NO LIF images shown in Fig. 5. It is seen from the images in Fig. 5 and spatial NO distribution in Fig. 6 that NO molecule concentration

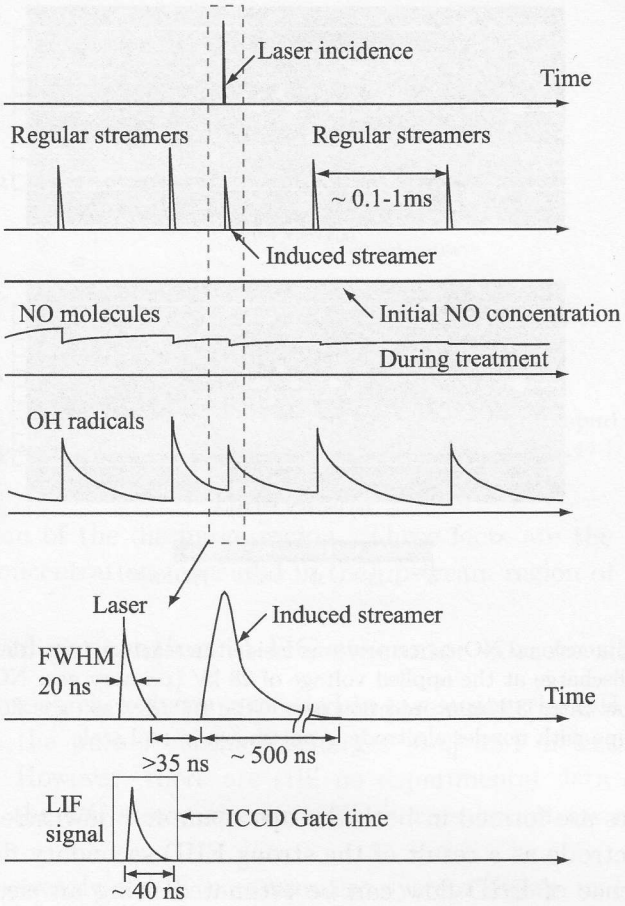

Figure 4. Schematic illustration of the time relationship between laser incidence, NO and OH LIF signals and laser-induced streamer when the laser beam was irradiated between the successive streamers during the steady-state discharge.

decreased not only in the plasma region created by the streamers but also in the upstream region of the discharge. In this experiment, the primary gas flow velocity is 4.2 mm/s. The gas flow in the reactor without the discharge is laminar by the estimation using the Reynolds number (R_e), which has been also confirmed by the LIF gas flow visualization using air containing NO [18]. However, the flow structure during the discharge results from the interaction between the primary flow, additional flow through the nozzles and secondary flow due to the ionic wind. It is considered that not only energetic electron induced plasma reaction occurs at the streamer head but also produced active radicals play an important role for NO removal in the reactor used in this study. Especially, the EHD flow is responsible for the enhanced NO removal far in the upstream region of the reactor. The

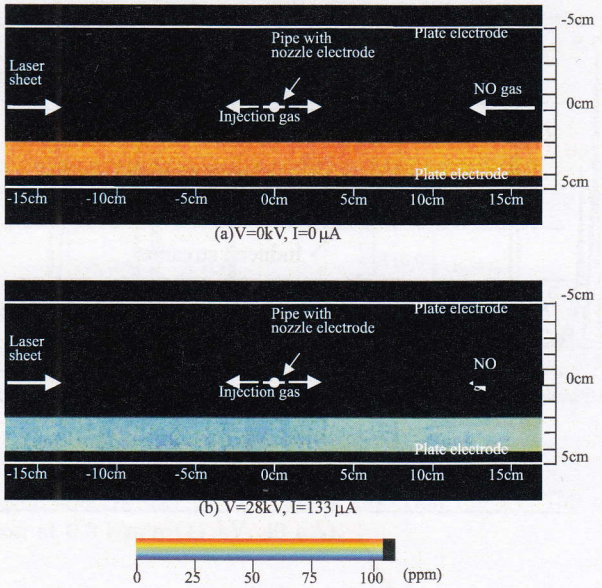

Figure 5. Two-dimensional NO concentrations inside the reactor. (a) without discharge and (b) with discharge at the applied voltage of 28 kV (primary gas: NO(100 ppm)/ dry air, gas flow rate: 3 l/min, injection gas: CO_2(9%)/dry air, gas flow rate: 0.44 l/min). The pipe with nozzles electrode is not shown in real scale.

strong vortexes are formed in both the upstream and downstream region around the nozzle electrode as a result of the strong EHD secondary flow [27, 28].

The influence of EHD flow can be estimated using an electrohydrodynamic number E_{hd} [29, 30] defined by

$$E_{hd} = \frac{J_p L^3}{\rho_g \nu^2 \mu_i}, \tag{1}$$

where J_p is the current density on the plate electrode, L is a characteristics length based on the reactor or stressed electrode dimension, ρ_g is the gas density, ν is the kinematic viscosity of the gas, μ_i is the positive ion mobility. The EHD number (E_{hd}) estimated for the typical operating condition is in the range of $10^6 - 10^8$ depending on J_p and L. While Reynolds number based on the reactor height is 40. Since the ratio E_{hd}/R_e^2 is much higher than 1, the ionic wind (EHD-induced secondary flow) becomes dominant [29, 30]. Therefore, the EHD-induced secondary flow in the present discharge system significantly influences the flow pattern inside the reactor (i.e. mixing of the gas occurs in the reactor). Particularly, ozone molecules produced by the streamer corona discharge in the corona radical shower reactor are observed not only in the downstream region but also in the upstream region of the reactor [27]. The EHD secondary flow is responsible for the ozone

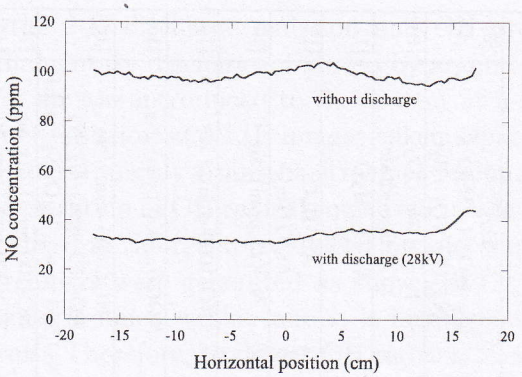

Figure 6. Spatial NO distributions as in Fig. 5. (primary gas: NO (100 ppm)/dry air, gas flow rate: 3 l/min, injection gas: CO_2(9%)/dry air, gas flow rate: 0.44 l/min).

transport upstream of the discharge region. These facts are the reason for the decrease of NO concentration measured in the upstream region of the reactor.

3.3 OH radical generation in DC streamer corona discharge

Recently, several researchers have succeeded in measuring the OH radicals using LIF technique in the pulsed corona discharges [5-9] and dielectric-barrier discharges [11, 12]. However, there are still no experimental data of OH radical concentrations in the DC streamer corona discharges except for our report [10] (see. Table I).

Using the time-resolved LIF measurement system shown in Fig. 1(b), it is found that the similar scheme to NO LIF can be applied for OH radical measurement (see, Fig. 4). During the steady-state discharge the ground-state OH ($X^2\Pi$) radicals produced in the one streamer is still present in the discharge region until the next streamers occur. Therefore, the measurement method based on no time synchronization between the streamer and laser pulse can be applied to the evaluation of DC streamer corona discharge. If we average the LIF signals, the steady-state measurement of OH radicals is also possible.

Table I. Use of LIF technique for the measurement of reactive species (OH, NO, O, N_2, N) in electrical discharges.

Observ. Species	Transition wavelength	Excitation (Detection)	Electrode system	Discharge type	Gas mixtures	Ref.
OH	$A^2\Sigma^+(v'=1) \leftarrow X^2\Pi\ (v''=0)$	282 nm (309 nm)	rod-rod electrode (gap 3 mm)	pulsed discharge	air	[5]
OH	$A^2\Sigma^+(v'=3) \leftarrow X^2\Pi(v''=0)$	248 nm (297 nm)	needle-plate electrode	pulsed discharge (gap 16 mm)	N_2/H_2O $N_2/O_2/H_2O$ $N_2/NO/H_2O$	[6] [7]
OH	$A^2\Sigma^+(v'=1) \leftarrow X^2\Pi(v''=0)$	282 nm	point-plane electrodes gap 9 mm	pulsed discharge	Ar/H_2O at I.P.	[8]
OH	$A^2\Sigma^+(v'=1) \leftarrow X^2\Pi(v''=0)$	285 nm (309 or 314 nm)	plate-plane electrodes (gap 10 mm)	pulsed discharge N_2	H_2O $NO/N_2/H_2O$ $N_2/O_2/VOC/H_2O$	[9]
OH	$A^2\Sigma^+(v'=1) \leftarrow X^2\Pi(v''=0)$	282 nm (309 nm)	nozzle-plane electrodes (gap 30 or 50 mm)	dc discharge	humid air/CO_2 NO/ humid air	[10]
OH	$A^2\Sigma^+(v'=1) \leftarrow X^2\Pi(v''=0)$	282 nm	DBD electrode (gap 2 mm)	silent discharge	$Ar/O_2/H_2O$	[11]
OH	$A^2\Sigma^+(v'=1) \leftarrow X^2\Pi(v''=0)$	282 nm (314 nm)	DBD electrode (gap 2 mm)	dielectric-barrier discharge	Air/H_2O $Ar/O/H_2O$	[12]
NO	$A^2\Sigma^+(v'=0) \leftarrow X^2\Pi(v''=0)$	226 nm (253 nm)	needle-plane electrodes (gap 7.3 mm)	pulsed discharge (negative polarity)	NO(25 ppm)/air	[13]
NO	$A^2\Sigma^+(v'=0) \leftarrow X^2\Pi(v''=0)$	226 nm (248 nm)	plate-plane electrodes (gap 10 mm)	pulsed discharge	NO(1000 ppm)/ N_2	[14]
NO	$A^2\Sigma^+(v'=0) \leftarrow X^2\Pi(v''=0)$	226 nm (254 nm)	needle-plane electrodes (gap 15 mm)	pulsed discharge	NO(30, 1000 ppm)/N_2	[15]
NO	$A^2\Sigma^+(v'=0) \leftarrow X^2\Pi(v''=0)$	226 nm	point-plane electrodes (gap 10 mm)	pulsed discharge	NO(1000 ppm)/N_2 NO(250 ppm)/O_2/N_2 NO(250 ppm)/H_2O/N_2; at I.P.	[16]
NO	$A^2\Sigma^+(v'=0) \leftarrow X^2\Pi(v''=0)$	226nm	nozzle-plane electrodes multiple nozzle-plane (gap 30 or 50 mm)	DC discharge	NO(100 ppm)/dry air NO(200 ppm)/dry air	[17] [18]
$O(^3P)$	$3p_2^3 \leftarrow 2p^3P_2$ TALIF	226nm (two photon) (845 nm)	DBD electrode (gap 7mm)	pulsed discharge	N_2/O_2	[19]
N_2 $(A^3\Sigma)$	$C^3\Pi_u \leftarrow B^3\Pi_g \leftarrow A^3\Sigma_u^+$ OODR-LIF	688, 350nm	point plane electrode (gap < 2 mm)	pulsed discharge	I.P.	[20]
$N(^4S)$	$3p^3S^0_{J=3/2} \leftarrow 3p^3gS^0$	207 nm (two photon) (745 nm)	pin-plate electrode	pulsed discharge	N_2; N_2/O_2	[21]

Abbrev.: I.P. – intermediate pressure; TALIF – two-photon absorption laser-induced fluorescence; OODR-LIF – optical-optical double resonance-LIF.

Figure 7 shows the 2-D discharge emission and OH profiles in the reactor under steady-state filamentary discharges induced by argon injection through the nozzle electrode. Wet air was introduced to the reactor at a flow rate of 3 l/min. Although the streamer emission and LIF images taken separately, it can be seen that OH LIF signal comes mainly from the streamer region. Consequently, it is considered that the generation of OH radicals occurred inside the streamer. When the discharge was realized in the reactor by CO_2/air injection through the nozzle electrode, spread streamers were generated as shown in Fig. 8(a). In this case, however, the LIF signal is much weaker and it is insufficient for single-shot 2-D imaging of OH radicals. Therefore, to detect OH radicals in streamers with flame like pattern, the laser beam, which was not expanded to the sheet, was used. In order to increase SN ratio of the image, the image shown in Fig. 8(b) is a sum of 10 captured images. The intensive part of the LIF signal corresponds to the region of streamers. In addition, OH LIF signal was observed outside the streamer region. This observation could be possible only when a special filter with a high transmittance for LIF signal (i.e., transmittance at 282 nm and 309 nm are less than 0.01% and ca. 90%, respectively.) was attached onto the lens of the ICCD camera. The reason for OH LIF signal outside the streamer region may be due to ozone interference in OH LIF measurement explained in later.

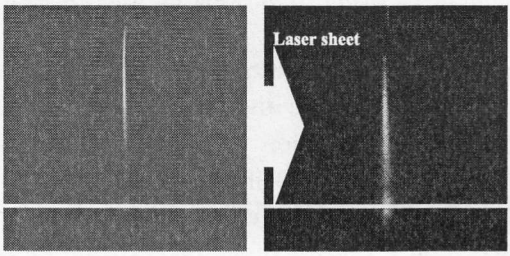

Figure 7. Comparison of (a) streamer (gate time 1 ms, sum of 5 images) and (b) OH LIF (gate time 50 ns, sum of 30 images) in the reactor during the steady-state positive DC corona with Ar injection. (V=12 kV, I=200 μA, primary gas: wet air, 3 l/min., injection gas: argon, 0.3 l/min.)

Although the plasma chemical reaction is not simple, the principal reactions for producing OH radial are expected as follows:

$$H_2O + e \rightarrow H + OH + e, \tag{R3}$$

$$O_2 + e \rightarrow O(^3P) + O(^1D) + e, \tag{R4}$$

$$O(^1D) + H_2O \rightarrow 2OH. \tag{R5}$$

In the discharge, it is well known that ozone is produced through the reaction

$$O + O_2 + M \rightarrow O_3 + M. \tag{R6}$$

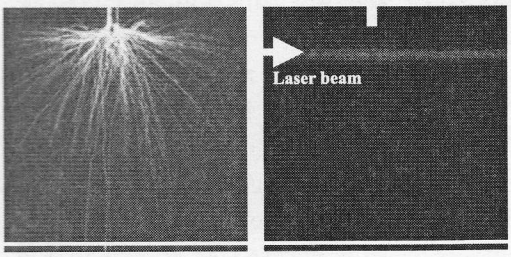

Figure 8. Comparison of (a) streamer (gate time 1 ms, sum of 5 images) and (b) OH LIF (gate time 50 ns, sum of 10 images) in the reactor during the steady-state positive DC corona without Ar injection. (V= 20 kV, I=50 μA, primary gas: wet air, 3 l/min., injection gas: CO_2, 0.15 l/min and air, 0.3 l/min.).

The produced OH is also reduced in the plasma:

$$OH + O \rightarrow H + O_2, \tag{R7}$$

$$OH + OH \rightarrow H_2O + O, \tag{R8}$$

$$OH + O_3 \rightarrow HO_2 + O_2. \tag{R9}$$

It is noted that the effects of other reactions should be taken into account for explaining the OH behaviour.

In another experiment on OH LIF measurement, we found that the OH LIF signal was detected after the stop of the discharge. And the OH LIF signal became weaker as a time elapsed. The detection time limit was almost equal to the gas residence time in the reactor. This may suggest that ozone, which has a long life time, is related to the formation of OH radical under the UV irradiation (in this case, probe laser beam). The UV laser dissociates ozone into $O(^1D)$ and O_2.

$$O_3 + h\nu(\lambda < 310 \text{ nm}) \rightarrow O(^1D) + O_2. \tag{R10}$$

OH radical is produced by the reaction R5 and is also contributed to OH LIF signal. The ozone/UV laser process has been observed in LIF measurement using the pulsed corona discharge [31]. This effect was also observed in our experiment during the steady-state DC corona discharge condition. Although we observed the decrease of OH LIF signal when the NO molecules are added into the primary humid air flow, the effect of OH radials on NO removal in DC streamer corona discharge is still in the line of research.

4 Conclusions

The laser-induced fluorescence technique was used for in-situ NO molecule and OH radical observation in DC streamer corona discharge. Under the steady-state

DC corona discharge condition, the timing between the streamer discharge pulse, LIF signal and laser-induced streamer was important for in-situ LIF measurement. Especially, separate recording of the LIF signal was possible by an appropriate adjusting of the recording delay and exposure time of the ICCD camera. NO removal due to oxidation occurs far from the discharge zone in the upstream of the reactor. In the present reactor at a low primary gas flow rate, EHD flow becomes to be dominant, and the flow towards the upstream affects the decrease of NO along the primary gas flow. While, it is confirmed that ground-state OH radicals were generated in DC streamer corona discharge. By comparing the images between the streamer corona discharge area and OH LIF profile, it is considered that OH radicals were generated in the streamers and its diffusion was almost negligible. A more detailed experiment is needed for considering OH radial role for gas treatment in DC streamer corona discharge.

Acknowledgment The author would like to express sincere thanks to Prof. T. Ohkubo, Prof. Y. Nomoto, Dr M. Kocik, Prof. J. Mizeraczyk, and Prof. J.S. Chang. The author would like to thank Prof. T. Oda, Prof. R. Ono, and Prof. F. Tochikubo for variable discussions and comments. This work was partially sponsored by Japan Society for Promotion of Science.

Received 20 November 2006

References

[1] Veldhuizen van E. M., and Rutgers W. R.: *Pulsed positive corona streamer propagation and branching*, J. Phys. D: Appl. Phys., 35 (2002), 2169-2179.

[2] Ono R., and Oda T.: *Formation and structure of primary and secondary streamers in positive pulsed corona discharge – effect of oxygen concentration and applied voltage*, J. Phys. D: Appl. Phys., 36 (2003), 1952-1958.

[3] Ohkubo T., Kanazawa S., Nomoto Y., Chang J. S., and Adachi T.: *NO_x removal by corona discharge in a pipe with nozzle electrode system*, IEEE Trans.Ind. Appl., 30 (1994), 856-861.

[4] Ohkubo T., Kanazawa S., Nomoto Y., Chang J. S., and Adachi T.: *Time dependence of NOx removal rate by a corona radical shower system*, IEEE Trans.Ind. Appl., 32 (1996), 1068-1062.

[5] Ershov A., and Borysow J.: *Dynamics of OH ($X^2\Pi, v = 0$) in high-energy atomospheric pressure electrical pulsed discharge*, J. Phys. D: Appl. Phys., 28 (1995), 68-74.

[6] Ono R., and Oda T.: *Meaurement of hydroxyl radicals in pulsed corona discharge*, J. Electrostatics, 55 (2002), 333-342.

[7] Ono R., and Oda T.: *Dynamics and density estimation of hydroxyl radicals in a pulsed corona discharge*, J. Phys. D: Appl. Phys., 35 (2002), 2133-2138.

[8] Tochikubo F., Uchida S., and Watanabe T.: *Study of decay characteristics of OH radical density in pulsed discharge in Ar/H_2O*, Jpn. J. Appl. Phys., 43 (2004), 315-320.

[9] Magne L., and Pasquiers S.: *LIF spectroscopy applied to the study of non-thermal plasmas for atmospheric pollutant abatement*, C.R. Physique, 6 (2005), 908-917.

[10] Kanazawa S., Tanaka H., Kajiwara A., Ohkubo T., Nomoto Y., Kocik M. Mizeraczyk J., and Chang J. S.: *LIF imaging of OH radicals in DC positive streamer coronas*, Thin Solid Films, (2006).

[11] Coogan J. J., and Sappey A. D.: *Distribution of OH within silent discharge plasma reactor*, IEEE Trans. Plasma Sci., 24 (1996), 91-92.

[12] Sankaranarayanan R., Pashaie B., and Dhali S. K.: *Laser-induced fluorescence of OH radicals in a dielectric barrier discharge*, Appl. Phys. Lett., 77 (2000), 2970-2972.

[13] Roth G. J., and Gundersen M. A.: *Laser-induced fluorescence images of NO distribution after needle-plane negative corona discharge*, IEEE Trans. Plasma Sci., 27 (1999), 28-29.

[14] Fresnet F., Baravian, Pasquiers S., Puech V., Rousseau A., and Rozoy M.: *Time-resolved laser-induced fluorescence study of NO removal plasma technology in NO/N_2 mixtures*, J. Phys. D: Appl. Phys., 33 (2000), 1315-1322.

[15] Hazama H., Fujiwara M., and Tanimoto M.: *Removal processes of nitric oxide along positive streamers observed by laser-induced fluorescence imaging spectroscopy*, Chem. Phys. Lett., 323 (2000), 542-548.

[16] Tochikubo F., and Watanabe T.: *Two-dimensional measurement of emission intensity and NO density in pulsed corona discharge*, HAKONE VII, (2000) 219-223.

[17] Kanazawa S., Ito T., Shuto Y., Ohkubo T., Nomoto Y., and Mizeraczyk J.: *Two-dimensional distribution of ground-state NO density by LIF technique in DC needle-to-plate positive streamer coronas during NO removal processing*, IEEE Trans. Ind. Appl., 37 (2001), 1663-1667.

[18] Kanazawa S., Sumi T., Shimamoto S., Ohkubo T., Nomoto Y., Kocik M., Mizeraczyk J., and Chang J.S.: *Diagnostics of NO oxidation process in a nonthermal plasma reactor: Features of DC streamer-corona discharge and NO LIF profile*, IEEE Trans. Plasma Sci., 32 (2004), 25-31.

[19] Ono R., Yamashita Y., Takezawa K., and Oda T.: *Behaviour of atomic oxygen in a pulsed dielectric barrier discharge measured by laser-induced fluorescence*, J. Phys. D: Appl. Phys., 38 (2005), 2812-2816.

[20] Dilecce G., Ambrico P.F., Debenedictis S.: Plasma Source Sci. Technol., 14 (2005), 561.

[21] Lukas C., Spaan M., Schulz-von der Gathen V., Thomson M., Wegst R., Dobele H. F., and Neiger M.: Plasma Source Sci. Technol., 10 (2001), 445.

[22] Kanazawa S., Ito T., Shuto Y., Ohkubo T., and Nomoto Y.: *Characteristics of laser-induced streamer corona discharge in a needle-to-plate electrode system*, J. Electrost., 55 (2002) 343-350.

[23] Ohkubo T., Ito T., Shuto Y., Akamine S., Kanazawa S., Nomoto Y., and Mizeraczyk J.: *Streamer corona discharge induced by laser pulses during LIF measurements in a dc non-thermal plasma reactor for NO oxidation*, J. Adv. Oxid. Technol., 5 (2002), 129-134.

[24] Ohkubo T., Kanazawa S., Nomoto Y., Kocik M., and Mizeraczyk J.: *Characteristics of DC corona streamers induced by UV laser irradiation in non-thermal plasma*, J. Adv. Oxid. Technol. 8 (2005), 218-225.

[25] Wang W., Wang S., Liu F., Zheng W., and Wang D.: Spectrochimica Acta Part A, 63 (2006), 477-482.

[26] Selzer P. M., and Wang Ch. C., J. Chem. Phys., 71 (1979)3786

[27] Dekowski J., Mizeraczyk J., Kocik M., Dors M., Podlinski J., Kanazawa S., Ohkubo T., and Chang J.S.: *Electrohydrodynamic flow and its effect on ozone transport in a corona radical shower reactor*, IEEE Trans. Plasma Sci., 32 (2004), 370-379.

[28] Dekowski J., Kocik M., Mizeraczyk J., Kanazawa S., Ohkubo T., and Chang J.S.: *Flow patterns in a wire (barbed with nozzles)-to-plate electrostatic precipitator model*, [in:] Proc. 2003 Annual Meeting of The Institute of Electrostatics Japan, 2003, 189-194.

[29] Chang J. S., and Watson A., Electromagnetic Hydrodynamics, *IEEE Trans. Elect. Insul.*, 5 (1994) 871-895.

[30] IEEE-DEIS-EHD Technical Committee, *Recommended International Standard for Dimensionless Parameters Used In Electrohydrodynamics*, IEEE Trans. Elect. Insul., 10 (2003), 3-6.

[31] Ono R., and Oda T.: *Dynamics of ozone and OH radicals generated by pulsed corona discharge in humid-air flow reactor measured by laser spectroscopy*, J. Appl. Phys, 93 (2003), 5876-5882.